Desalination and Water Treatment
www.deswater.com

doi: 10/5004/dwt.2012.2959

Taylor & Francis
Taylor & Francis Group

45 (2012) 324–330
July

Beaded $ZnTiO_3$ fibers prepared by electrospinning and their photocatalytic properties

Chengcheng Zhang[a], Xiang Li[a], Tian Zheng[a], Yang Yang[a], Yongxin Li[a], Ye Li[a], Ce Wang[a,*], Lijuan Li[b]

[a]*Jilin University Alan G MacDiarmid Institute, Changchun 130012, PR China*
Tel./Fax: +86 431 85168292; email: cwang@jlu.edu.cn
[b]*Department of Chemistry and Biochemistry, California State University, Long Beach, CA 90840, USA*

Received 10 May 2011; Accepted 17 January 2012

ABSTRACT

Beaded $ZnTiO_3$ fibers have been fabricated by a combination of sol-gel, electrospinning and calcination techniques. The $ZnTiO_3$ can be obtained by calcining at 700°C for 3.5 h. The morphology and structure of the obtained photocatalytic material were characterized by various analytical techniques such as scanning electron microscopy (SEM), transmission electron microscope (TEM), energy dispersive X-ray spectroscopy (EDX), Fourier transform infrared (FT-IR) and X-ray diffraction (XRD). Their photocatalytic activity was evaluated by the decomposition of methyl violet dye solution under simulated solar light irradiation. The fibers exhibited a beaded-like morphology as shown in the TEM image. The effect of different morphology including fibers and short fibers on the photocatalytic performance was also investigated. For the $ZnTiO_3$ fibers and short fibers, almost all the dyes were degraded after 4 h and 3 h, respectively.

Keywords: Sol-gel; Electrospinning; Calcination; Methyl violet; Photocatalytic degradation; $ZnTiO_3$

1. Introduction

In the past decade, with the development of industries, the detrimental effects of environmental contamination due to dyes and pigments are becoming more and more serious. As a result, considerable attention has been focused on effective purification methods for the treatment of the dyes and pigments. However, the existing methods like adsorption or biological treatment appear to have many drawbacks, since the former involves only phase transfer of the pollutants without degradation, and the latter cannot be applied to contaminants which are toxic or refractory to the bacteria [1]. This leads to the investigation of another effective, pollution-free and low cost method. Solar energy, an inexhaustible natural energy source, could be widely applied for color removal and organic degradation of the dyes and pigments. Recently, among all the photocatalysts, the role of metal oxide photocatalysts such as titanium oxide and zinc oxide is becoming more and more important since they have some advantages over other materials [1–8].

TiO_2 and ZnO are both wideband semiconductors with excellent properties and extensive applications, which have attracted much interest on either single material [9,10] or ZnO–TiO_2 composites [11–15]. There are five compounds in ZnO–TiO_2 binary oxide system, that is, $ZnTiO_3$ (cubic, hexagonal), Zn_2TiO_4 (cubic, tetragonal) and $Zn_2Ti_3O_8$ (cubic) [16]. Among them, $ZnTiO_3$ is a promising candidate as a paint pigment [17], catalytic

*Corresponding author.

sorbent for the desulfurization of hot coal gases [18], and gas sensor for the detection of ethanol, CO, etc. [19]. $ZnTiO_3$ also has potential applications as a photocatalysis material [16]. Synthesis of $ZnTiO_3$ from 1ZnO and $1TiO_2$ by solid-state reaction method is very difficult because it tends to decompose into Zn_2TiO_4 and rutile during solid-state reaction process. There are several methods to prepare $ZnTiO_3$, such as the solid-state reaction method [20], sol–gel process [21], and molten salt synthesis [22], etc. Here we use electrospinning, a simple and convenient method to prepare $ZnTiO_3$ fibers.

The electrospinning method was first developed in the 1930s [23] and is a fabrication process of fibers from elongation of polymer solutions under a high electrical field. A variety of polymers can be electrospun to form uniform fibers. Recently, it has been demonstrated that electrospinning and controlled calcination can be combined to provide a simple route to prepare one-dimensional inorganic semiconductor fibers, such as TiO_2 [24–27], ZnO [28] and SnO_2 [29], etc. The fibers prepared by electrospinning have good orientation, large specific surface area, large aspect ratio, and dimensional stability, which can be applied in tissue engineering [30], desalination [31], sensing [32] as well as catalysis [33].

In this paper, beaded $ZnTiO_3$ fibers were prepared with a combination of sol-gel, electrospinning and calcination technique. The photocatalytic properties of electrospun beaded fibers in the photochemical degradation of methyl violet dye solution under simulated solar light irradiation were first investigated, though the $ZnTiO_3$ fibers have been already produced by electrospinning technique [34,35]. And, we also discussed the effect of different morphology including long beaded fibers and short beaded fibers on the photocatalytic performance. The morphology and structure of the obtained photocatalytic material were characterized by various analytical techniques such as scanning electron microscopy (SEM), transmission electron microscope (TEM), energy dispersive X-ray spectroscopy (EDX), Fourier transform infrared (FT-IR) and X-ray diffraction (XRD).

2. Experimental

2.1. Materials

Tetrabutyl titanate {$[CH_3(CH_2)_3O]_4Ti$, ≥98%, CP} was purchased from China Huishi Biochemistry Chemical Company. Absolute ethanol (GR), acetic acid (GR) zinc nitrate hexahydrate [$Zn(NO_3)_2 \cdot 6H_2O$, AR] and methyl violet were supplied by Beijing Chemical Reagent Plant. N, N-dimethylformamide (DMF, AR) was purchased from Tianjin Tiantai Chemical Factory. Polyvinylpyrrolidone (PVP, $M_W \approx 1{,}300{,}000$) was purchased from Aldrich. All the above chemicals were used as received without further purification.

2.2. Synthesis

The precursor sol for electrospinning was prepared in the following procedures. In a typical synthesis, 0.3816 g $Zn(NO_3)_2 \cdot 6H_2O$ was dissolved into a solution of 1.555 g absolute ethanol and 1.422 g DMF under vigorous stirring for 10 min. Subsequently, this solution was added drop-wise into the mixture of 1 g acetic acid and 2 g absolute ethanol that contained 0.51 g PVP and 0.4375 g $[CH_3(CH_2)_3O]_4Ti$ to give a spinnable sol. The solution was delivered to a glass syringe (inner diameter: about 1 mm, outer diameter: about 1.5 mm). As a high voltage of 15 kV was applied, the solution jet accelerated towards the cathode, which was placed 15 cm from the needle tip, leading to the formation of fiber arrays onto the substrate accompanied by partial solvent evaporation. The operating flow rate was 0.30–0.40 mlh^{-1}.

The as-spun fibers were calcined at 700°C for 3.5 h in air with a heating rate of 4°C min^{-1} to completely eliminate the organics. After natural cooling to room temperature, the fibers were ground to obtain short fibers. Then, the fibers and short fibers were denoted as LF and SF, respectively.

2.3. Characterization

Thermogravimetric analysis (Pyris1 TGA) was conducted in air atmosphere over the temperature region 100–800°C at a heating rate of 10°C min^{-1} with 5.2 mg as-spun fibers. The structures of the samples were characterized by X-ray diffraction (XRD) equipment (Siemens D5005 diffractometer using Cu Kα radiation λ = 1.5418 Å; step size 0.05°, time per step 0.2 s, 50 kV, 150 mA) in the scan range 2θ between 20° and 80°. IR spectra were obtained on a fourier transform infrared spectrometer (FT-IR, BRUKER VECTOR 22) with a resolution of 4 cm^{-1}; KBr wafers were used, and the weight percentage of fibers in KBr was about 0.7%.The morphologies of the samples were observed by scanning electron microscopy (SEM, SHIMADZU SSX-550) and transmission electron microscope (TEM, JEM-2000EX). A small section of the fibers was placed on the SEM sample holder and sputter coated with gold to take the SEM photographs. TEM sample was prepared by ultrasonically dispersing the obtained fibers after calcination at 700°C in ethanol for 1 min and then placing one or two drops of the suspension onto a C-coated, Cu grid (230 mesh). After evaporation of the ethanol, the sample was ready for TEM analysis. The fiber diameter range was determined by taking measurements 100 points from SEM images using Nano Measurer, 1.2.0.0 (Department of chemistry, Fudan University, China). EDX analysis was done using a SEM coupled to an X-ray detector. UV–vis absorption spectra were recorded on a UV-2501 PC Spectrometer (wavelength range: 190–900 nm; wavelength

accuracy: ±0.4 nm) with a resolution of 0.1 nm. N_2 adsorption-desorption of the fibers was measured on a Micromeritics Gemini V at liquid nitrogen temperature of 77 K after degassing of the samples at 150°C for 2 h under vacuum. The specific surface area was calculated by the Brunauer–Emmett–Teller (BET) method in the range of relative pressures between 0.05 and 0.30. The pore width was calculated from the adsorption and desorption branches of the isotherms using the Barrett–Joyner–Halenda (BJH) method.

2.4. Photocatalytic activity measurements

The photocatalytic activities of the beaded $ZnTiO_3$ fibers on the photooxidation of methyl violet were investigated in a quartz photochemical reactor. A 500 W Xenon lamp (CHFXQ500W, 14,200 LX) was used as the light source to simulate solar light. A fan was used to cool down the lamp. Throughout the experiment, the temperature of the reaction solution changed little [36]. In the photocatalytic degradation of methyl violet solution using $ZnTiO_3$ as photocatalyst system, the degradation rate was higher at alkaline pH values and increased as pH increasing from 4 to 8. When the pH value was 8, the maximum degradation rate was achieved [16]. Here the pH values were kept at 6.2 in all the reactions to eliminate the effect of the pH value on methyl violet reduction. In each reaction, the sample with the weight of 0.025 g was added to 25 ml methyl violet solution with a concentration of 10 mg l^{-1}. The suspension was magnetically stirred in the dark for 1 h to reach the adsorption–desorption equilibrium on the photocatalyst surface. After illumination, 1 ml mixture solution was taken from the suspension followed by centrifugation and filtration at the 1 h intervals. Finally a clear solution was obtained. The change of absorption at 581 nm (–N=N–) was monitored to identify the concentration of methyl violet using a UV–vis spectrophotometer.

The concentration of methyl violet being linearly proportional to the intensity of the absorption peak at 581 nm, the decomposition efficiency of methyl violet can be calculated using the following equation:

$$\eta = \frac{C_0 - C}{C_0} = \frac{A_0 - A}{A_0} \times 100\% \quad (1)$$

where C_0 and A_0 are the equilibrium concentration and absorbency of methyl violet solution at 581 nm corresponding to maximum absorption wavelength; C and A are the concentration and absorbency after simulated solar light irradiation at homologous time.

We also calculated the reaction rate constant by using a pseudo-first-order equation [Eq. (2)] [37].

$$\ln(\frac{C_0}{C}) = kt \quad (2)$$

where C_0 is the equilibrium concentration of the dye (mg l^{-1}), C is the concentration of the dye at time t (mg l^{-1}), t is the irradiation time, k is the reaction rate constant (h^{-1}).

3. Results and discussion

Thermogravimetric (TG) measurement was utilized to analyze the thermal decomposition characteristics of the precursor fibers of $ZnTiO_3$ in air atmosphere in the temperature range of 100–800°C, as shown in Fig. 1. The TG curve can be divided into four main weight loss stages. The first 7% of weight loss occurred below 240°C can be attributed to the evaporation of water and trapped solvents, such as ethanol, N, N-dimethylformamide and acetic acid. The following significant weight loss of 53% which occurs in the temperature range of 240–330°C results from the combustion and decomposition of PVP [38]. The third weight loss of 17% in the temperature range of 330–700°C results from the dehydroxylation of Ti–OH into TiO_2 and decomposition of the NO_3 group [21]. In the final step over 700°C, no weight loss can be observed, which indicates that the inorganic fibers have been obtained.

The morphology of the electrospun fibers before and after calcination was examined using SEM. Fig. 2a shows the typical SEM image of fibers by electrospinning precursory sol. These fibers were randomly distributed on the substrate, even and smooth. They were longer than several millimeters, with diameters between 100 nm and 500 nm. As shown in Fig. 2b, after annealing the sample in air at 700°C, a well-defined fiber texture kept unchange with the shrinking of the fibers to a range of 50–200 nm in diameter due to the removal of organic substances. The detailed morphology and structure of the sample were further characterized and analyzed by TEM. Clearly seen from the TEM image, $ZnTiO_3$ fibers

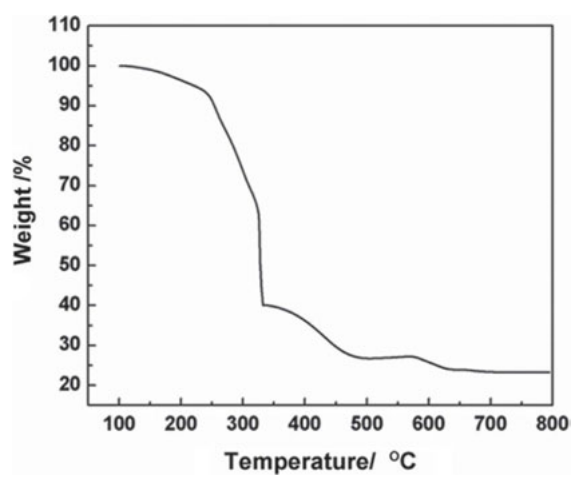

Fig. 1. The TG curve of $ZnTiO_3$ precursor fibers.

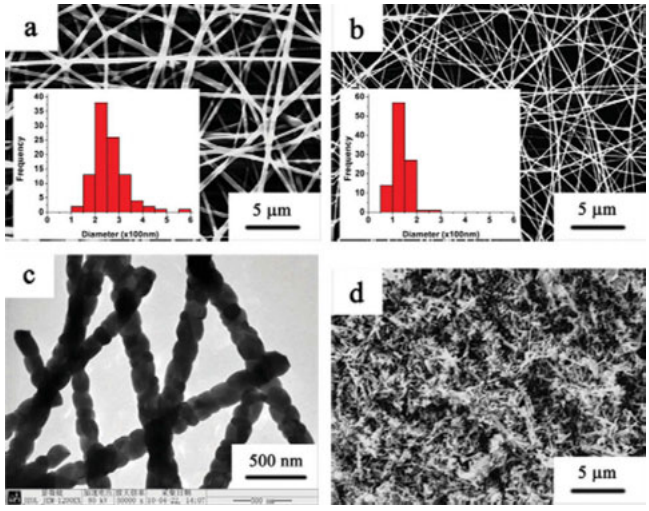

Fig. 2. SEM images of as-spun $[CH_3(CH_2)_3O]_4Ti/Zn(NO_3)_2$/PVP fibers before (a) and after (b) calcined at 700°C for 3.5 h in air. Inset: the graphics with the diameter size values, respectively. (c) TEM image of $ZnTiO_3$ fibers. (d) SEM image of $ZnTiO_3$ short fibers ground from the fibers.

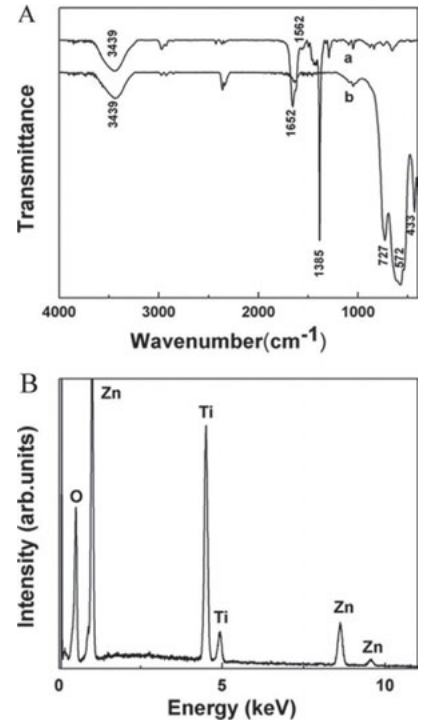

Fig. 3. (A) FTIR spectra of as-spun $[CH_3(CH_2)_3O]_4Ti/Zn(NO_3)_2$/PVP fibers before (a) and after (b) calcination at 700°C for 3.5 h. (B) EDX spectrum of $ZnTiO_3$ fibers.

had a rough surface and consisted of many nanoparticles with large grain size to form beaded-like morphology (Fig. 2c). This nanochain morphology is a polycrystalline nanowire with more defects or lattice imperfections due to the larger surface-to-volume ratio, which is beneficial to the photocatalytic activity of the $ZnTiO_3$ fibers [39]. Fig. 2d shows the SEM image of $ZnTiO_3$ short fibers ground from the fibers. As shown in the image, the length-diameter ratio of the short fibers was reduced steeply and partial short fibers were agglomerated due to the high surface energy, resulting in lower BET surface area (5.77 m^2g^{-1}) than that (12.43 m^2g^{-1}) of the $ZnTiO_3$ fibers [40,41].

Fig. 3A shows the FT-IR spectra of the sample before and after calcination at 700°C. In the case of the composite fibers before calcination [Fig. 3A(a)], bands at about 1652 cm^{-1} are resulted from the vibration of C =O groups of PVP [27]. The peaks at about 1562 and 1385 cm^{-1} are due to the N–O bond vibration of NO_3^- [21]. Generally, the bands in the low-wave number region (600–650 cm^{-1}) are assigned to Ti–O bond vibrations [21]. However, the characteristic peaks of PVP and NO_3^- have disappeared after calcining at 700°C for 3.5 h, which indicated that the polymers and NO_3^- had been degraded [Fig. 3A(b)]. At the same time, the absorption bands of the Zn–O stretching vibrations appeared at 433 cm^{-1} [42] and bands at 727 and 572 cm^{-1} were ascribed to Ti–O stretching vibrations in the TiO_6 group [21]. Moreover, the composition of the fibers was characterized by EDX spectrum shown in Fig. 3B. The presence of Zn, O, and Ti elements and no other impurity peaks occurring indicate that after calcination, the organic components have been degraded.

Due to TiO_6 group existing in all forms of $ZnTiO_3$, $Zn_2Ti_3O_8$, and Zn_2TiO_4, to further confirm the structure of the fibers, XRD spectrum was conducted. Fig. 4 shows XRD spectrum of the fibers calcined at 700°C. The peaks at 2θ values of 23.80°, 32.66°, 35.20°, 40.35°, 48.83°, 53.31°, 56.74°, 61.70°, 63.28°, 68.64°, 70.87°,74.59°and 79.59°observed in the sample are indicative of correspond

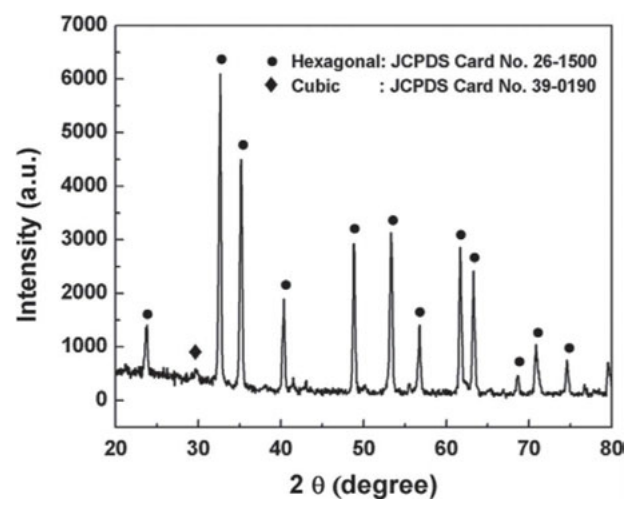

Fig. 4. XRD patterns of $ZnTiO_3$ fibers after calcination at 700°C for 3.5 h.

diffraction peaks at (102), (104), (110), (113), (204), (205), (108), (214), (300), (208), (1010), (220) and (218) respectively, which can be perfectly indexed to a typical hexagonal structure of $ZnTiO_3$ (JCPDS Card No. 26-1500) with a trace of cubic $ZnTiO_3$ at 2θ value of 29.62°(JCPDS Card No. 39-0190).

Fig. 5 shows the adsorption behaviors and photocatalytic activities of beaded $ZnTiO_3$ fibers evaluated by the degradation of methyl violet solution. As a comparison, the degradation with only the fibers in the dark or with only simulated solar light irradiation without the fibers was also measured. In the absence of simulated solar light irradiation, only small concentration changes were observed due to small adsorption (Fig. 5a). The direct photolysis of dyes in the absence of fibers was examined via simulated solar light irradiation of aqueous dye solutions. The results show that dye methyl violet (10 mg l^{-1}) decomposed just a little after 4 h of simulated solar light irradiation (Fig. 5b). However, the absorption of methyl violet at 581 nm almost disappeared after the methyl violet solution was irradiated for 4 h in the presence of beaded $ZnTiO_3$ fibers (Fig. 5c). In addition, no new absorption band arose in the UV-vis region, indicating the breakdown of the chromophore. These experiments demonstrated that both solar light and a photocatalyst, such as $ZnTiO_3$ were needed for the effective destruction of methyl violet. The photocatalytic degradation of organic dye is initiated by photoexcitation of the semiconductor, followed by the formation of an electron-hole pair on the surface of catalyst. The dye can undergo direct oxidation to reactive intermediates by the high oxidative potential of the hole (h^+_{VB}) [43]. High reactive hydroxyl radicals can also be formed, either by the decomposition of water or by the reaction of the hole with OH^-. The hydroxyl radical, an extremely strong, non-selective oxidant can partially or completely oxidize several organic chemicals [43]. The band gap of the hexagonal-phase $ZnTiO_3$ is 3.05 eV, which indicates that the hexagonal-phase $ZnTiO_3$ has a larger potential redox than the anatase phase TiO_2 (3.2 eV) for the photocatalytic degradation of methyl violet with simulated solar light irradiation [16]. In order to further investigate the effect of different morphology including LF and SF for photocatalysis, we have also studied the photocatalytic activity of $ZnTiO_3$ SF. It was found that for the beaded $ZnTiO_3$ SF, the photodegradation rate of methyl violet was faster and after only 3 h, the dye achieved nearly total degradation (Fig. 5d). We attribute the higher activity

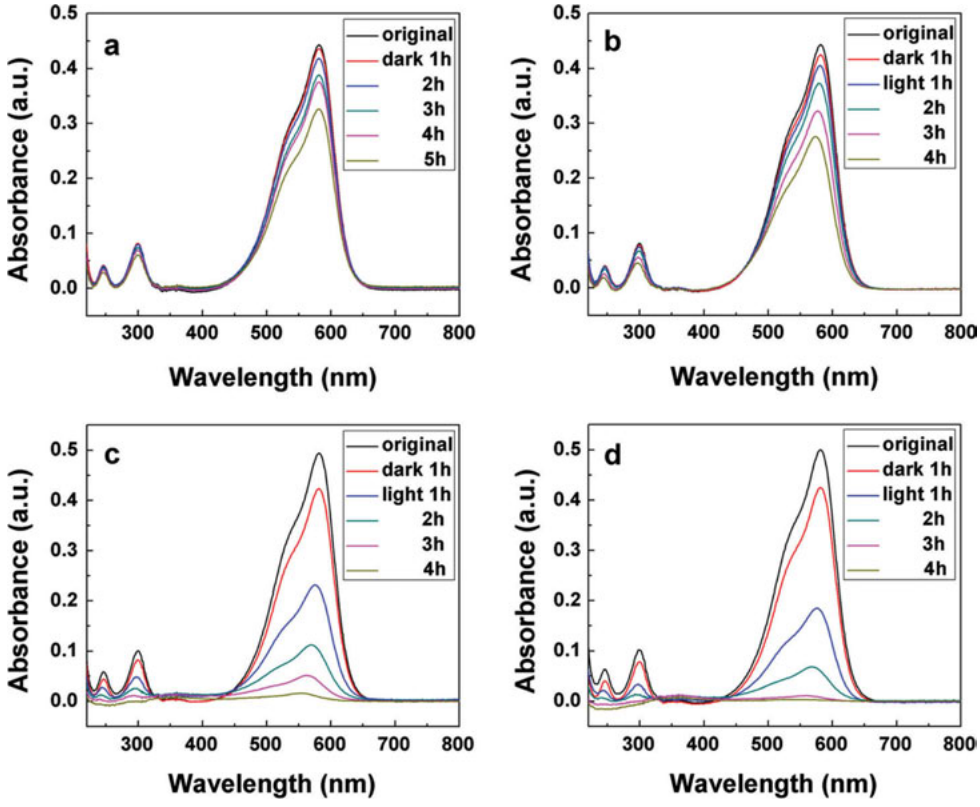

Fig. 5. The UV–vis spectra of the methyl violet solution at pH = 6.2 during simulated solar light irradiation in the presence of the fibers calcination at 700°C for 3.5 h: (a) with only the LF in the dark, (b) with only simulated solar light irradiation without the fibers, (c) beaded $ZnTiO_3$ LF, and (d) beaded $ZnTiO_3$ SF.

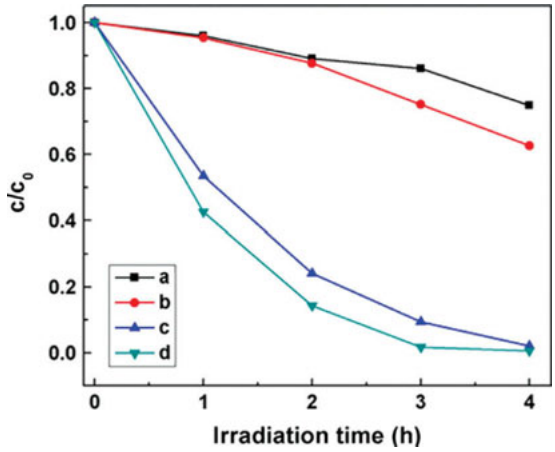

Fig. 6. Photocatalytic decomposition of methyl violet solution at pH = 6.2 during simulated solar light irradiation in the presence of the fibers calcination at 700°C for 3.5 h: (a) with only the LF in the dark, (b) with only simulated solar light irradiation without the fibers, (c) beaded $ZnTiO_3$ LF, and (d) beaded $ZnTiO_3$ SF.

of the $ZnTiO_3$ SF to the pore structures. The pore structural characteristics of the $ZnTiO_3$ LF and the SF were analyzed by the nitrogen adsorption and desorption techniques. The fibers had voids between fibers and surface pores. The dye molecule can first diffuse into voids in short time and then, finally diffuse into surface pores in long time [37]. The $ZnTiO_3$ SF had more voids due to short length-diameter ratio with larger average pore width (74.5 ± 9.5 nm) than the LF (52.4 ± 4.6 nm). Therefore, though the $ZnTiO_3$ SF had smaller BET surface area (5.77 m^2g^{-1}) than that (12.43 m^2g^{-1}) of the $ZnTiO_3$ LF, the adsorption of dye on the $ZnTiO_3$ SF was larger than that on the $ZnTiO_3$ LF, resulting in the higher photocatalytic activity.

Fig. 6 shows the kinetics of methyl violet photodegradation. After 2 h of simulated solar light irradiation, about 76% dye was degraded by the $ZnTiO_3$ LF. In contrast, 86% degradation occurred in the case of the $ZnTiO_3$ SF, which was faster than the photocatalysts reported [44,45]. After calculating from Eq. (2), we found that the degradation rate (k = 1.119 h^{-1}) of $ZnTiO_3$ SF was higher than that (0.771 h^{-1}) of $ZnTiO_3$ LF. So $ZnTiO_3$ SF is better photocatalysts than $ZnTiO_3$ LF.

4. Conclusions

In conclusion, we have successfully prepared beaded $ZnTiO_3$ fibers by a combination of sol-gel, electrospinning and calcination techniques. The fibers exhibit $ZnTiO_3$ crystallization after calcining at 700°C for 3.5 h. These $ZnTiO_3$ fibers with a beaded-like morphology have high solar light photocatalytic activity toward decomposition of methyl violet. After 4 h of simulated solar light irradiation, the absorption of methyl violet at 581 nm almost disappeared. In order to further investigate the effect of the morphology and nanostructure for photocatalysis, we also studied the photocatalytic activity of the $ZnTiO_3$ SF ground from the LF. And for the $ZnTiO_3$ SF, almost all the dyes were degraded after only 3 h. The photocatalytic characteristics of the $ZnTiO_3$ SF are superior to those of the $ZnTiO_3$ LF. We propose that the $ZnTiO_3$ fibers be suitable for the degradation of organic pollutants.

Acknowledgements

The work has been supported by National 973 Project (No. 2007CB936203 and S2009061009), NSF China (No. 50973038), National 863 Project (No. 2007AA03Z324) and Graduate Innovation Fund of Jilin University (No. 20111030).

References

[1] E. Evgenidou, K. Fytianos and I. Poulios, Semiconductor-sensitized photodegradation of dichlorvos in water using TiO_2 and ZnO as catalysts, Appl. Catal., B Environ., 59 (2005) 81–89.
[2] S.C. Pillai, P. Periyat, R. George, D.E. McCormack, M.K. Seery, H. Hayden, J. Colreavy, D. Corr and S.J. Hinder, Synthesis of high-temperature stable anatase TiO_2 photocatalyst, J. Phys. Chem. C, 111 (2007) 1605–1611.
[3] A. Muruganandham, N. Shobana and A. Swaminathan, Optimization of solar photocatalytic degradation conditions of Reactive Yellow14 azo dye in aqueous TiO_2, J. Mol. Catal. A: Chem., 246 (2006) 154–161.
[4] S.K. Kansal, A.H. Ali and S. Kapoor, Photocatalytic decolorization of biebrich scarlet dye in aqueous phase using different nanophotocatalysts, Desalination, 259 (2010) 147–155.
[5] S. Sakthivel, B. Neppolian, M.V. Shankar, B. Arabindoo, M. Palanichamy and V. Murugesan, Solar photocatalytic degradation of azo dye: comparison of photocatalytic efficiency of ZnO and TiO_2, Sol. Energy Mater. Sol. Cells, 80 (2003) 65–82.
[6] M. Muruganandham, N. Sobana and M. Swaminathan, Solar assisted photocatalytic and photochemical degradation of Reactive Black 5, J. Hazard. Mater., 137 (2006) 1371–1376.
[7] S.K. Pardeshi and A.B. Patil, Solar photocatalytic degradation of resorcinol a model endocrine disrupter in water using zinc oxide, J. Hazard. Mater., 163 (2009) 403–409.
[8] B. Krishnakumar, K. Selvam and R. Velmurugan, Influence of operational parameters on photodegradation of Acid Black 1 with ZnO, Desalin. Water Treat., 24 (2010) 132–139.
[9] B. Liu and E.S. Aydil, Growth of oriented single-crystalline rutile TiO_2 nanorods on transparent conducting substrates for dye-sensitized solar cells, J. Am. Chem. Soc., 131 (2009) 3985–3990.
[10] X.J. Feng, L. Feng, M.H. Jin, J. Zhai, L. Jiang and D.B. Zhu, Reversible super-hydrophobicity to super-hydrophilicity transition of aligned ZnO nanorod films, J. Am. Chem. Soc., 126 (2004) 62–63.
[11] J.Y. Park, S.W. Choi, J.W. Lee, C.M. Lee and S.S. Kim, Synthesis and gas sensing properties of TiO_2–ZnO core-shell nanofibers, J. Am. Ceram. Soc., 92 (2009) 2551–2554.
[12] M.A. Kanjwal, N.A.M. Barakat, F.A. Sheikh, S.J. Park and H.Y. Kim, Photocatalytic activity of ZnO-TiO_2 hierarchical nanostructure prepared by combined electrospinning and hydrothermal techniques, Macromol. Res., 18 (2010) 233–240.

[13] S.H. Hwang, J.Y. Song, Y.J. Jung, O.Y. Kweon, H. Song and J. Jang, Electrospun ZnO/TiO_2 composite nanofibers as a bactericidal agent, Chem. Commun., 47 (2011) 9164–9166.
[14] R.L. Liu, H.Y. Ye, X.P. Xiong and H.Q. Liu, Fabrication of TiO_2/ZnO composite nanofibers by electrospinning and their photocatalytic property, Mater. Chem. Phys., 121 (2010) 432–439.
[15] M.E. Fragalà, I. Cacciotti, Y. Aleeva, R. Lo Nigro, A. Bianco, G. Malandrino, C. Spinella, G. Pezzotti and G. Gusmano, Core–shell Zn-doped TiO_2–ZnO nanofibers fabricated via a combination of electrospinning and metal–organic chemical vapour deposition, Cryst. Eng., 12 (2010) 3858–3865.
[16] J.Z. Kong, A.D. Li, H.F. Zhai, H. Li, Q.Y. Yan, J. Ma and D. Wu, Preparation, characterization and photocatalytic properties of $ZnTiO_3$ powders, J. Hazard. Mater., 171 (2009) 918–923.
[17] A.T. McCord and H.F. Saunder, U.S. Patent 2739019, Ceram. Abstr., 1945, 24, 155.
[18] S. Ozdemir and T. Bardakci, Hydrogen sulfide removal from coal gas by zinc titanate sorbent, Sep. Purif. Technol., 16 (1999) 225–234.
[19] H. Obayashi, Y. Sakurai and T. Gejo, Perovskite-type oxides as ethanol sensors, J. Solid State Chem., 17 (1976) 299–303.
[20] A. Chaouchi, S. d'Astorg, S. Marinel and M. Aliouat, $ZnTiO_3$ ceramic sintered at low temperature with glass phase addition for LTCC applications, Mater. Chem. Phys., 103 (2007) 106–111.
[21] L. Hou, Y. Hou, M. Zhu, J. Tang, J.B. Liu and H. Wang, Formation and transformation of $ZnTiO_3$ prepared by sol–gel process, Mater. Lett., 59 (2005) 197–200.
[22] X. Xing, C. Zhang, L. Qiao, G. Liu, and J. Meng, Facile preparation of $ZnTiO_3$ ceramic powders in sodium/potassium chloride melts, J. Am. Ceram. Soc., 89 (2006) 1150–1153.
[23] A. Formhals, U.S. Patent Specification, 1975504, 1934.
[24] D. Li and Y.N. Xia, Fabrication of titania nanofibers by electrospinning, Nano Lett., 3 (2003) 555–560.
[25] I. Cacciotti, A. Bianco, G. Pezzotti and G. Gusmano, Synthesis, thermal behaviour and luminescence properties of rare earth-doped titania nanofibers, Chem. Eng. J., 166 (2011) 751–764.
[26] I. Cacciotti, A. Bianco, G. Pezzotti and G. Gusmano, Terbium and ytterbium-doped titania luminescent nanofibers by means of electrospinning technique, Mater. Chem. Phys., 126 (2011) 532–541.
[27] H.Y. Wang, Y. Wang, Y. Yang, X. Li and C. Wang, Photoluminescence properties of the rare-earth ions in the TiO_2 host nanofibers prepared via electrospinning, Mater. Res. Bull., 44 (2009) 408–414.
[28] X.H. Yang, C.L. Shao and H.Y. Guan, Preparation and characterization of ZnO nanofibers by using electrlospun PVA/zinc acetate composite fiber as precursor, Inorg. Chem. Commun., 7 (2004) 176–178.
[29] Z.J. Wang, Z.Y. Li, H.N. Zhang and C. Wang, Improved photocatalytic activity of mesoporous ZnO–SnO_2 coupled nanofibers, Catal. Commun., 11 (2009) 257–260.
[30] G.E. Wnek, M.E. Carr, D.G. Simpson and G.L. Bowlin, Electrospinning of nanofiber fibrinogen structures, Nano Lett., 3 (2003) 213–216.
[31] K.Y. Jea, S.H. Sang and L.J. Suk, Desalination properties of a novel composite membrane prepared by electrospinning method, Desalin. Water Treat., 15 (2010) 84–91.
[32] Z.Y. Li, H.N. Zhang and W. Zheng, Highly sensitive and stable humidity nanosensors based on LiCl doped TiO_2 electrospun nanofibers, J. Am. Chem. Soc., 130 (2008) 5036–5037.
[33] Y. Yang, H.Y. Wang, X. Li and C. Wang, Electrospun mesoporous W^{6+}-doped TiO_2 thin films for efficient visible-light photocatalysis, Mater. Lett., 63 (2009) 331–333.
[34] Z.Y. Cai, J.S. Li and Y.G. Wang, Fabrication of zinc titanate nanofibers by electrospinning technique, J. Alloys Compd., 489 (2010) 167–169.
[35] R. Ramaseshan and S. Ramakrishna, Zinc titanate nanofibers for the detoxification of chemical warfare simulants, J. Am. Ceram. Soc., 90 (2007) 1836–1842.
[36] L. Zhang, Y.M. He, Y. Wu and T.H. Wu, Photocatalytic degradation of RhB over $MgFe_2O_4$/TiO_2 composite materials, Mater. Sci. Eng. B, 176 (2011) 1497–1504.
[37] S.J. Doh, C. Kim, S.G. Lee, S.J. Lee and H. Kim, Development of photocatalytic TiO_2 nanofibers by electrospinning and its application to degradation of dye pollutants, J. Hazard. Mater., 154 (2008) 118–127.
[38] A.F. Lotus, S.N. Tacastacas, M.J. Pinti, L.A. Britton, N. Stojilovic, R.D. Ramsier and G.G. Chase, Fabrication and characterization of TiO_2–ZnO composite nanofibers, Physica E, 43 (2011) 857–861.
[39] M. Dutta and D. Basak, A novel and simple method to grow beaded nanochains of ZnO with superior photocatalytic activity, Nanotechnology, 20 (2009) 475602 (7 pp.).
[40] H. Liu, D. Wexler and G.X. Wang, One-pot facile synthesis of iron oxide nanowires as high capacity anode materials for lithium ion batteries, J. Alloys Compd., 487 (2009) L24–L27.
[41] E. Rabkin, G. Gottstein and L.S. Shvindlerman, Why do crystalline nanoparticles agglomerate with low misorientations? Scripta Mater., 65 (2011) 1101–1104.
[42] M.Z. Zheng, R.B. Yu, J. Chen, J. Zhao, G.R. Liu, X.R. Xing and J. Meng, Synthesis and characterization of (Zn,Cd)TiO_3 by a modified sol–gel method, J. Am. Ceram. Soc., 91 (2008) 544–547.
[43] N. Daneshvar, D. Salari and A.R. Khataee, Photocatalytic degradation of azo dye acid red 14 in water on ZnO as an alternative catalyst to TiO_2, J. Photochem. Photobiol., A Chem., 162 (2004) 317–322.
[44] C. Hachem, F. Bocquillon, O. Zahraa and M. Bouchy, Decolourization of textile industry wastewater by the photocatalytic degradation process, Dyes Pigm., 49 (2001) 117–125.
[45] F. Xia, E.C. Ou, L. Wang and J.Q. Wang, Photocatalytic degradation of dyes over cobalt doped mesoporous SBA-15 under sunlight, Dyes Pigm., 76 (2008) 76–81.